Hindawi
Geofluids
Volume 2022, Article ID 1213215, 17 pages
https://doi.org/10.1155/2022/1213215

Research Article

Experimental Investigation on Long-Term Strength and Acoustic Emission Characteristics of Coal Pillar under Inclined Compression Loading

Chong Li,[1,2,3] **Sifeng He**,[1,2] **and Zhijun Xu**[1,2]

[1]*School of Mines, China University of Mining and Technology, Xuzhou 221116, China*
[2]*Key Laboratory of Deep Coal Resource Mining, Ministry of Education, China University of Mining and Technology, Xuzhou 221116, China*
[3]*Laboratory of Mine Earthquake Monitoring and Prevention, Jiangsu Province, China University of Mining and Technology, Xuzhou 221116, China*

Correspondence should be addressed to Zhijun Xu; tb20020034b0@cumt.edu.cn

Received 17 November 2021; Revised 1 December 2021; Accepted 14 March 2022; Published 1 April 2022

Academic Editor: Fazhi Yan

Pillar rheological failure is one of the important reasons to induce earthquake, surface collapse, and water inrush disaster in underground mining engineering. Pillar is generally present under an inclined state and is significantly influenced by combining compression and shear loading. However, many scholars regard the long-term strength of coal or rock mass under pure uniaxial compression loading as the main evolution index of pillar strength, which is not consistent with engineering practice. In this paper, a new inclined uniaxial compression strength (IUCS) test system was developed and then used to carry out the IUCS test and creep test of coal specimens combined with an acoustic emission (AE) technology at various inclination angles (0°, 5°, 10°, 15°, and 20°). The variation of time-dependent deformation, peak strength, long-term strength (LTS), creep fracture model, and AE behavior of the coal with the inclination angels were discussed in detail. The results indicated that the peak strength and LTS of the coal nonlinearly decreased with the inclination angle increasing. The proportion of the peak strength to the LTS had remained constant between 58.5% and 62.9%, which can be considered as the inherent properties of coal rock. The creep failure model of the coal was transformed from tension-splitting failure at the inclination angle of 0° and 5° to tension-shear failure at the inclination angle of 10°-20°, which revealed that the inclination angles were favorable to the initiation and propagation of shear cracks. No matter any inclination angles, AE events can be divided into quiet period, low amplitude rising period, and high amplitude rising period with the periodic mutation of multistage loading points. Moreover, the cumulative AE energy gradually decreases with the increase of the inclination angles, which indicated that the shear stress caused by the specimen inclination can make crack initiation and propagation with less energy absorption. The research results will assist in the long-term strength design and time-dependent stability assessment of the coal pillar.

1. Introduction

Coal pillar, as a common engineering structure in underground mining engineering, has made critical contribution to control the ground subsidence and water intrusion prevention [1, 2]. Moreover, coal pillar can also be used as the support systems to ensure the stability of mining roadway and safety of mine worker. Recently, the construction of underground reservoir has become an extremely important method for realizing the water resource preservation during mining in northwest of China, where the coal pillar is the main component of underground reservoir as the water barrier [3–5], as shown in Figure 1. Hence, it is necessary to comprehensively investigate the long-term strength (LTS) and macroscopic-microscopic fracture behavior of coal pillar for optimizing the strength design. In most previous studies, the pure uniaxial compression strength (UCS) was used to evaluate the bearing capacity of pillar, which is

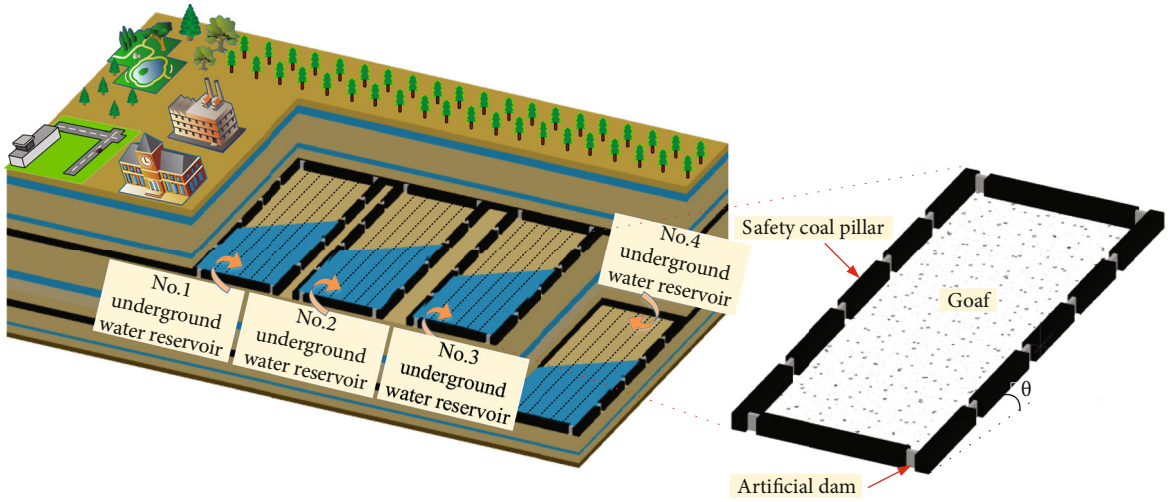

Figure 1: Schematic diagram of underground reservoir structure.

inconsistent with the practice engineering condition [6–9]. Numerous geological surveys have shown that many pillars generally had a certain inclination angle. As a result, the axial direction of pillar is not parallel to the direction of maximum principal stress and a shear stress component will occur in this situation, which make the specimens in a state of combining compression and shear stress. However, Chen, Pariseau, and Das et al. have noted that the shear stress component is beneficial to crack initiation and propagation of coal rock and can weaken the strength of pillar, which should be considered for designing the strength of pillars [10–12]. Furthermore, some researchers have also pointed out that the strength and fracture characteristics of pillar are closely related to the creep behaviors [13–15], which cannot be ignored in the strength design of pillar. Therefore, a comprehensive understanding of the creep mechanical and failure behavior of coal rock under different inclination angles is extremely important in mining.

Creep phenomenon reflects the time-dependent deformation characteristics of coal rock under a constant loading below their peak strength. Many researchers have done a large number of creep tests of coal in order to better understand the instability characteristics of coal pillar. Those creep tests mainly focused on the reports of uniaxial compression or confined compression loading conditions, which are unable to reflect the creep mechanical response of coal pillar under inclined compression test condition [16–18]. However, numerous studies suggested a significant impact of shear stress caused by inclination angle on pillar stability. By considering the shear effect, Pariseau [11] and Foroughi and Vutukuri [19] improved the formula for assessing pillar safety and concluded that shear loadings could weaken the stability of pillars. The research by Suorineni et al. [20] indicated that pillar strength decreases with the increase of inclination angles, proposing the limitation of conventional empirical equations in pillar design. For investigating the relationship between inclination angle and UCS of coal, He and Chen et al. [21–23] developed a combined compression and shear test (C-CAST) system and performed a series of uniaxial compression tests on coal specimens under various inclination angles. The experimental results showed that the strength experienced a decrease with inclination angles enlarging, and the coal specimens were prone to shear failure at a large inclination angle. Wu et al. [24] also carried out the inclined UCS test of coal specimens by using the C-CAST system, finding that the UCS of coal specimens can reach to their maximum at 5° inclination angle and then gradually decrease with the increasing inclination angle. The above studies demonstrated that the inclination angle has an extremely important effect on the strength of coal pillar, which should be considered in the design of pillar strength.

To more effectively reveal the LTS and creep fracture mechanism of coal pillar under inclined compression loading, this paper conducts a set of inclined uniaxial compression strength (IUCS) tests and creep tests on coal specimens under various inclination angles using the IUCS test system and then analyzes the impact of inclination angles on creep deformation curve, LTS, and creep failure model. The acoustic emission (AE) technique is also introduced to investigate the characteristics of AE energy released in specimen creep failure under various inclination angles and to support a discussion over the mechanism of inclination angle effect on creep cracking. The outcomes of this paper are expected to provide theoretical references for the LTS design and stability assessment of inclined coal pillars occurring in complicated geological condition.

2. Materials and Methods

2.1. Materials. The coal specimens were sampled from Changzhi City, Shanxi Province, China, and then cored into cylinders of 100 mm height and 50 mm diameter, with both ends polished for a better flatness. The sampling location and tested specimens are shown in Figures 2 and 3, respectively. In Figure 4, the XRD results show that calcite and amorphous are the main mineral composition of the tested samples. Before performing creep tests, the quality, diameter, height, and wave velocity of specimens were tested.

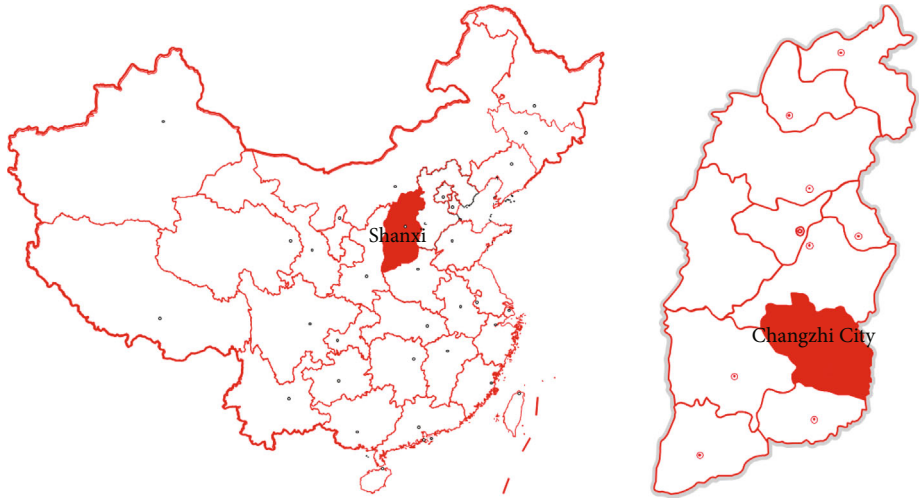

Figure 2: Sampling site of specimens to be tested.

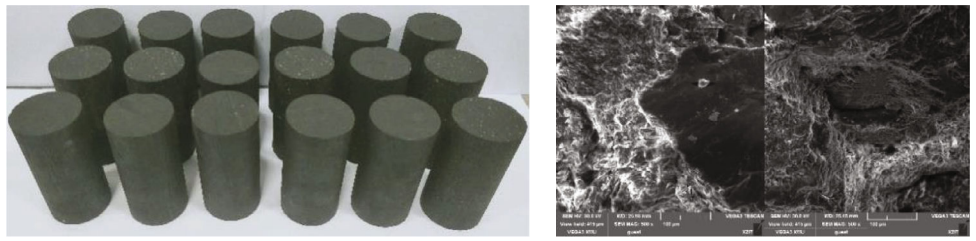

(a) (b)

Figure 3: Standardized coal specimens and microstructure profile.

Finally, the specimens with 1050 m/s in wave velocity and 1.27 g/cm^3 in average density were chosen for the creep test. Figure 3(b) shows the scanning electron microscopy (SEM) results, indicating that the selected samples have good compaction and uniformity, which can reduce the test error caused by the sample structure.

2.2. IUCS Test System. Figure 5 shows the configuration of the IUCS test system. This system is composed of two identical adapters on the top and bottom, respectively. A rotatable calibration device, fixed connection device, and a fixing screw device are the main components of an adapter. The angle scale attached to the rotatable calibration device can fix the inclination degree designed for each specimen. Before testing, the specimen is placed between the top and bottom adapters, and then, the IUCS test system is fixed onto the material testing system (MTS). The AE system is used to monitor the energy signals released by specimens, with four type RS-54A probes and 300 kHz resonant frequency. Relevant parameters are set as preamplifier being 40 dB and threshold value 40 dB, respectively. The peak definition time (PDT), hit definition time (HDT), and hit lockout time (HLT) are also set as 50 μs, 100 μs, and 500 μs, respectively [10]. In addition, the four probes are pasted onto the surface of tested specimens using a couplant (hot-melt adhesive), which can help to collect acoustic emission signals better. The installation position is shown in Figure 5(a).

2.3. UCS and IUCS Comparative Analysis. Figure 6 shows the stress and deformation state of the specimen before and after the test under different loading methods. As shown in Figure 6, the external loading force is parallel to the specimen axis in the traditional UCS test. However, there is an angle θ between the external loading force and specimen axis in the inclined UCS test. Hence, a shear stress component will occur in the IUCS test system, which does not exist in the traditional UCS test. This result will make the specimens in a state of combining compression and shear stress. In this case, the axial stress component, shear stress component, and axial strain of specimens can be expressed as [13]

$$\begin{aligned} \sigma_\theta &= \frac{F\cos\theta}{A}, \\ \varepsilon_\theta &= \frac{\chi}{d}, \\ \tau_\theta &= \frac{F\sin\theta}{A}, \end{aligned} \tag{1}$$

where σ_θ and ε_θ refer to the axial stress component and axial strain, τ_θ is the shear stress component, F is the vertical force posed by MTS on the ends, A and d are the cross-sectional area and the initial height of specimens, respectively. χ is the platen displacement. It should be noted that the IUCS test system exists certain end effect due to the existence of groove inside the rotatable calibration device, but

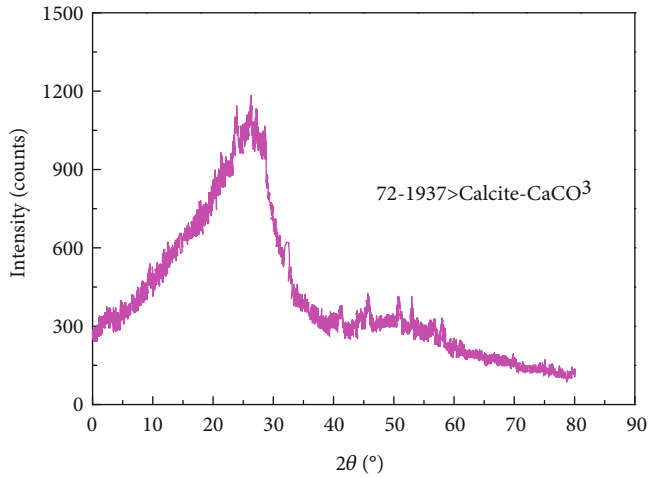

Figure 4: XRD-based composition analysis of coal specimens.

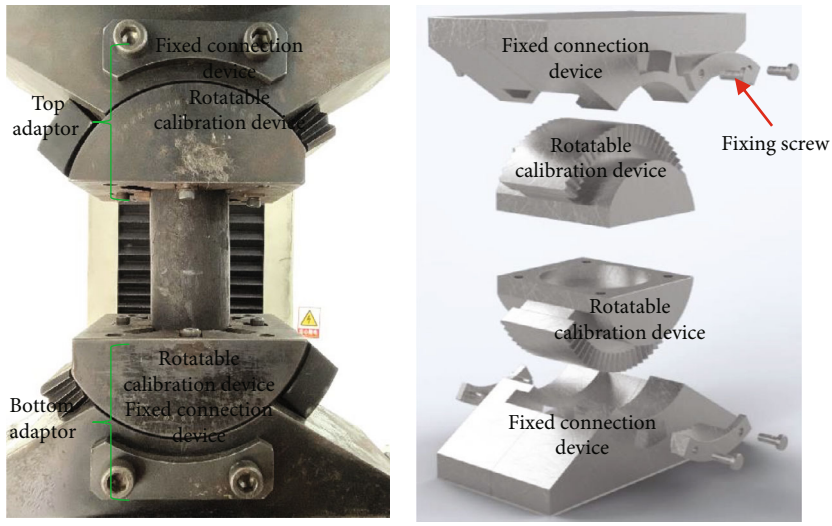

(a) (b)

Figure 5: Configuration of the IUCS test system: (a) real products' picture; (b) schematic diagram [23].

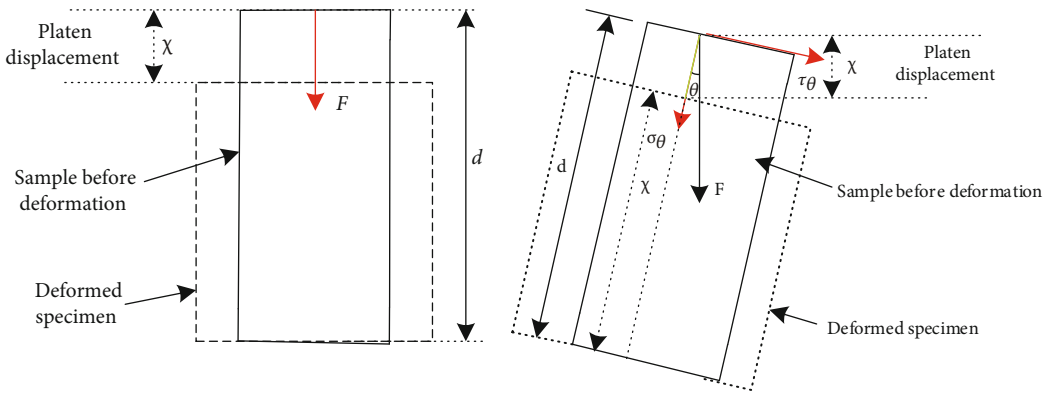

(a) Traditional UCS test (b) IUCS test

Figure 6: Stress and deformation state of the specimen before and after the test [2].

Table 1: The UCS of coal specimens under various inclination angles.

Inclination angles		UCS (MPa)	Selected UCS (MPa)	Average UCS (MPa)	Absolute deviation (MPa)	Relative deviation (%)	Standard deviation (MPa)	Relative standard deviation (%)
0°	1#	11.24	/	15.55	/	/	0.288	1.85
	2#	16.07	16.07		0.52	3.3		
	3#	15.32	15.32		0.23	1.5		
	4#	17.78	/		/	/		
	5#	15.26	15.26		0.29	1.9		
5°	1#	8.65	/	9.73			0.095	0.98
	2#	9.89	9.89		0.16	1.6		
	3#	13.54	/					
	4#	9.35	9.35		0.38	3.9		
	5#	9.95	9.95		0.22	2.3		
10°	1#	7.9	7.9	7.46	0.44	5.9	0.037	0.5
	2#	7.16	7.16		0.3	4.02		
	3#	8.9	/					
	4#	6.9	/					
	5#	7.32	7.32		0.14	1.9		
15°	1#	7.5	/	5.82			0.015	0.26
	2#	5.1	/					
	3#	5.42	5.42		0.4	6.9		
	4#	6.21	6.21		0.39	6.7		
	5#	5.83	5.83		0.01	0.2		
20°	1#	5.9	/	4.71			0.002	0.04
	2#	3.57	/					
	3#	4.89	4.89		0.18	3.8		
	4#	4.67	4.67		0.04	0.8		
	5#	4.57	4.57		0.14	2.97		

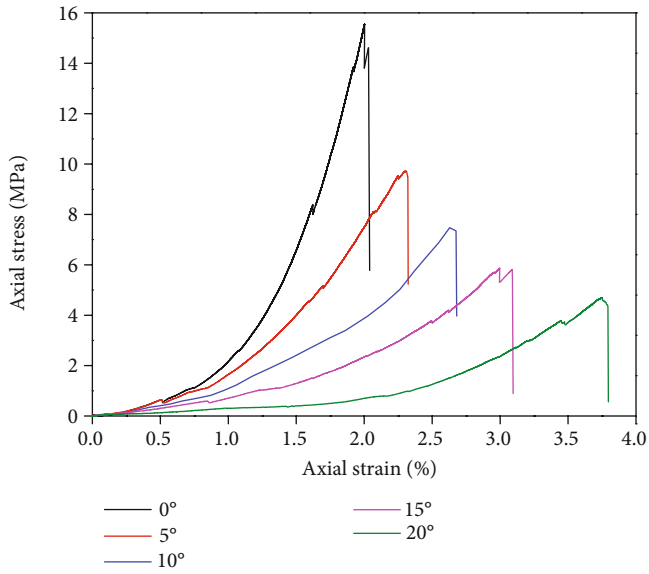

Figure 7: Stress-strain curves of coal specimens under various inclination angles.

less affected the experimental results, which has been verified in literature [21–23].

2.4. Methods and Procedures of Creep Tests. The methods and procedures of creep tests are as follows:

(i) IUCS test system installation and loading procedures: Step 1: rotate the rotatable calibration device to the designed inclination angle, and fix it using screws. Then, place a specimen on the central groove of the calibration device (the bottom adapter), and fix it through accessories. Finally, move the IUCS test system onto the MTS. Step 2: operate MTS to load slowly till the specimen is about to touch the top adapter, and then, start the preloading. When the prestress reaches 0.1 kN, the loading process ceases automatically. Repeat this process till the specimen is completely fixed. Then, perform the follow-up tests

(ii) UCS tests under various inclination angles: after installing the IUCS test system, UCS tests on coal specimens under various inclination angles are conducted to quantify specimen UCS and provide parametric references for creep test design. Five different inclination angles are designed, ranging from 0° to 20°, with an interval of 5°; each angle is tested five times, marked from 1# to 5#. Only three UCS by removing the maximum and minimum values are chosen for analyzing under each angle. In the UCS test, the specimens are loaded by incremental external stress, and the loading rate is set as 0.5 MPa/s. Due to the limitations of the test system, it is difficult to exclude the large experimental error caused by the horizontal slip dislocation of bottom adaptor when the inclination angle exceeds 25° [24]. Hence, in order to the accuracy of experimental results, the variation range of inclination angle is set as 0°-20°

(iii) Uniaxial creep tests with various inclination angles: based on the results of UCS tests, the uniaxial peak strength of coal specimens under different inclination angles is obtained. According to these results, we design six loading stages for the creep test, with each stage sustaining 12 h. The multistage loading method is selected as the stress path of the test process under five inclination angles. As the previous UCS tests, creep tests are conducted under five different inclination angles, and each angle is performed five times. The testing schemes are as follows. Step 1: install the IUCS test system and AE signal acquisition system. The probes are attached to the surface of specimens using couplant (hot-melt adhesive). Step 2: start preloading at a rate of 3 mm/min. The loading is automatically stopped as the prestress reaches 0.1 kN. Repeat this process till the specimen is completely fixed. Step 3: perform creep tests and AE signal acquisition tests simultaneously under a loading rate of 0.1 MPa/s. After reaching a stress loading level of 17%σ_{max}, this value is held for approximately 12 hours, followed by a stress loading level of 33%σ_{max}. Step 4: repeat Step 3 to complete the stress loading level from 33%σ_{max} to 95%σ_{max} till the specimen creep failure occurs, during which the data of each test system should be well recorded and stored. After creep test, the LTS, creep fracture model, and AE date of coal specimens will be systematically analyzed and discussed under different inclination angles

3. Results and Analysis

3.1. Impact of Inclination Angle on the Peak Strength. Table 1 gives the detailed UCS of coal specimens under different inclination angles. It shows that the standard deviation of the UCS changes between 0.002 MPa and 0.288 MPa, while the relative deviation changes between 0.04% and 1.85%, meaning that the experimental data is rational [2]. Thus, a typical stress-strain curve of each inclination angle is chosen and plotted in Figure 7. It shows that the stress-strain curve of any inclination angle consists of four stages: the pore compaction stage, approximate linear elastic stage, nonlinear cracking stage, and postpeak drop stage. Besides that, each curve shows a rapid decline at the fourth stage, indicating that brittle failure behavior is evident under every inclination angle. Additionally, the uniaxial peak strength declines with the increase of inclination angle. Specifically, the UCS is 9.73 MPa, 7.46 MPa, 5.82 MPa, and 4.71 MPa under the angle of 5°, 10°, 15°, and 20°, respectively, dropping by 37.4%, 52%, 62.6%, and 69.7% compared with the scenario of 0° inclination angle. The reason is that the shear stress generated by the inclined specimen aggravates the initiation and propagation of internal cracks, leading the specimen favor to failure even under lower compressive loading [25–29].

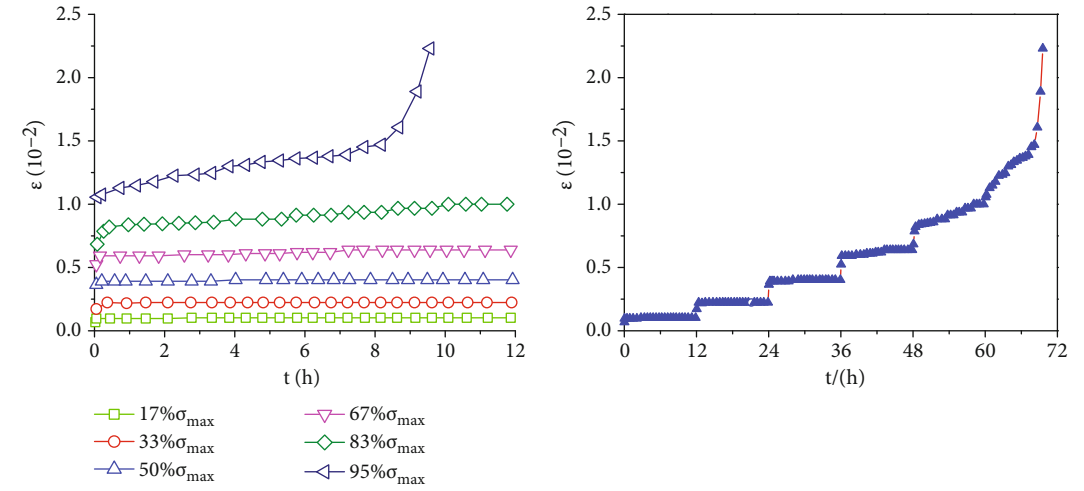

(a) 0°

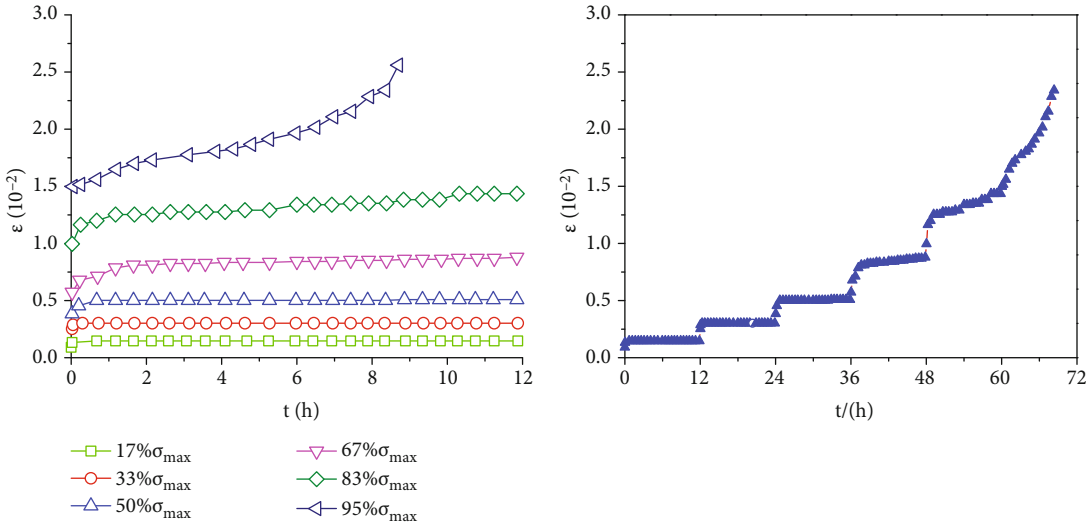

(b) 5°

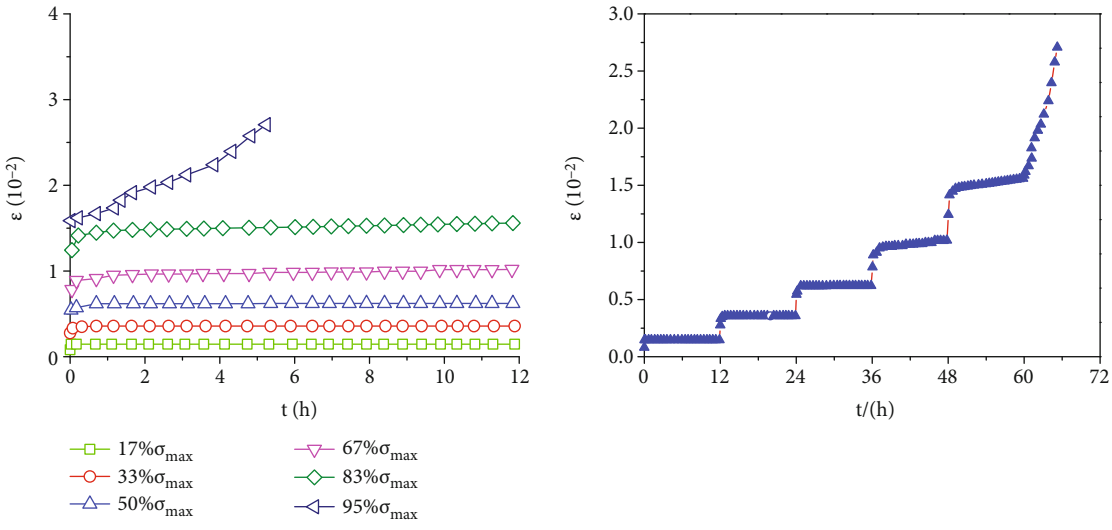

(c) 10°

Figure 8: Continued.

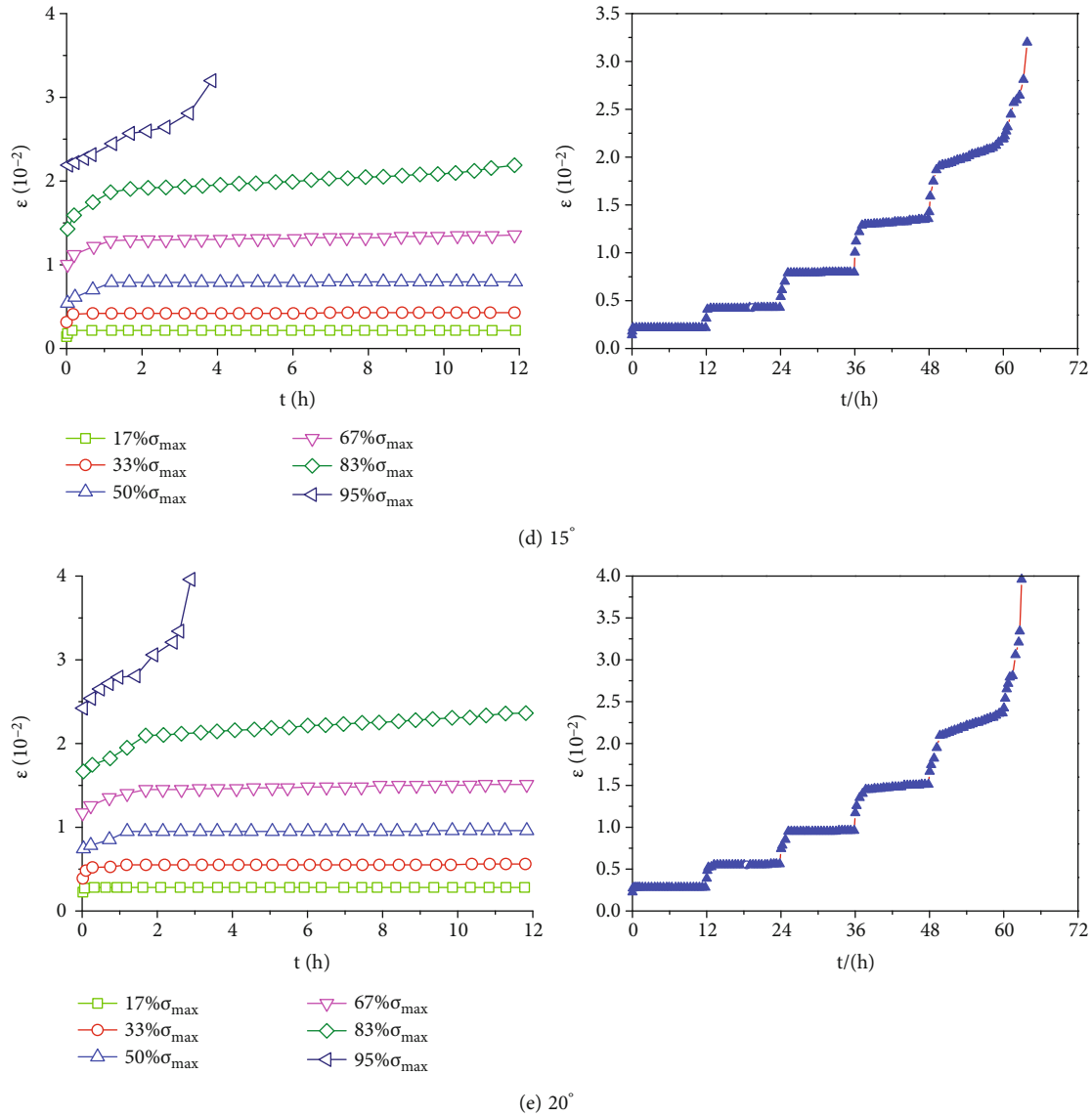

(d) 15°

(e) 20°

Figure 8: Axial strain-time creep curve of coal specimens under various inclination angles.

3.2. Impact of Inclination Angles on Creep Curve and Deformation. Figure 8 gives the axial creep curves under various inclination angles. It can be found that the axial creep strain increased with the increasing loading levels. Besides, the time-dependent deformation is more evident with increased external stress levels. However, the axial creep strain characteristics are the same at any inclination angles. At low creep stress levels (i.e., the stress level is below 83%σ_{max}), the time-dependent deformation curves have only two creep stages: the primary stage with a decreased strain rate and the steady creep stage with a constant strain rate. At the last creep stress level (i.e., the level is 95%σ_{max}), the creep curves under different inclination angles show three creep stages: the primary stage, the steady creep stage, and the accelerated creep stage, after which the specimens got failed.

Figure 9(a) shows that creep curves at the last creep stress level (95%σ_{max}) differ from various inclination angles. It can be found that the critical accelerated creep strain increases linearly with the increase of inclination angles, while the creep time when specimens fail decreases linearly. Besides, the creep strain rate at the last loading level is shown in Figure 9(b). It indicates that the inclination angles significantly impact the creep strain rate when the loading level is 95%σ_{max}. Actually, the creep strain rate increases particularly significantly under more inclined angles, i.e., under the angle of 15° and 20°. It means that the propagation and penetration of cracks tend to be faster under higher inclination angles.

3.3. Impact of Inclination Angles on LTS of Coal Specimens. Previous research showed that the LTS of rock mass is lower than its UCS. Additionally, the instability of rock structures such as coal pillars is relative with time. Thus, the LTS is an essential mechanical parameter reflecting the time-dependent characteristics of rock masses [30, 31]. At

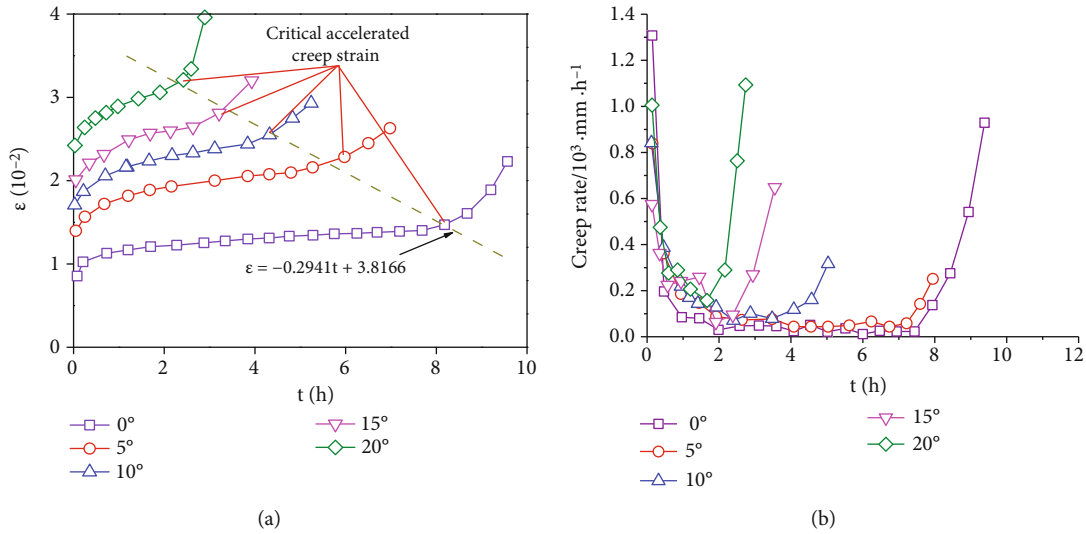

(a) (b)

FIGURE 9: Axial strain-time creep curve and deformation rate of coal specimens for stress loading level of 95%σ_{max} under various inclination angles.

present, there are three main methods to determine the LTS of coal rock: isochronous stress-strain curves method, transition creep method, and the inflection point of the steady creep rate method [32, 33]. Among these methods, the isochronous stress-strain curve method is the most widely used, which will be used in this study to obtain the LTS of coal specimens under various inclination angles.

The isochronous stress-strain curves give the relationship between the creep stress and strain at the same duration, as shown in Figure 10. Actually, the curves under each inclination angle have a bifurcation point where the corresponding stress is defined as the LTS of coal rock. Table 2 shows the LTS value of coal mass at various inclination angles. As shown in Table 2, the standard deviation of the LTS changes between 0.02 MPa and 0.08 MPa, while the relative deviation changes between 0.1% and 2.52%, meaning that the experimental data is rational. In addition, there is an obvious quadratic negative correlation between the LTS and inclination angle. The decrease rate of the LTS also decreases with increasing inclination angles. For instance, when the inclination angle varies from 0° to 10°, the LTS attenuates from 9.58 MPa to 4.65 MPa by 4.93 MPa. However, when the inclination angle varies from 15° to 20°, the LTS attenuates from 3.66 MPa to 2.96 MPa by 0.70 MPa. Hence, the inclination angle is adverse to the LTS of coal pillars, which can be considered in the LTS design of coal pillars. Moreover, according to Tables 1 and 2, the average proportion of the peak strength to the LTS of coal specimen had remained constant between 58.5% and 62.9%, which can be considered as the inherent properties of coal rock.

3.4. Creep Failure Modes of Coal Specimens. Figure 11 shows the pictures of coal specimens after creep tests. To further analyze the failure modes, Figure 11 also gives the sketches of propagation cracks and detached block of the failed specimens under different inclination angles. When the inclination angle is 0°, the broken specimens have several tensile cracks approximately parallel to the loading direction and few shear cracks, as shown in Figure 11(a). The failure mode under this inclination angle is mainly tensile splitting with localized shear sliding, and the broken specimens are relatively complete. When the inclination angle is 5°, the failure specimens have several tensile cracks and some shear cracks with an angle of the specimen axis, as shown in Figure 11(b). The failure mode under this inclination angle is still tensile splitting with localized shear sliding, while the broken specimens exist with few caved coal fragments. When the inclination angle is between 10° and 20°, main cracks extend with an angle, which is larger than that under the 5° scenario, of the loading direction, as shown from Figures 11(c)–11(e). The failure model under this inclination angle is mainly shear sliding along with tensile splitting, and the broken specimens are fractured. The testing results indicate that inclination angles significantly impact the creep failure modes and the degree of fragmentation specimens. In all, the failure modes gradually transform from the pure tensile-splitting mode to a combination of both splitting and shear sliding with increasing inclination angles.

3.5. AE Response of Coal Specimens in Creep Process to Various Inclination Angles. During the initiation, propagation, and penetration of cracks, coal rocks can release large amounts of energy in stress waves, which can be collected by the AE technique. Therefore, the evolution of microcracking processes can be effectively detected by monitoring the AE signals emitted by coal specimens during creeping. Figure 12 compares the time-dependent variation of the AE energy, accumulative AE energy, and creep deformation of coal specimens under different inclination angles. Figure 13 shows the relationship between the accumulative AE energy and time or inclination angle, respectively. The following can be found from Figures 12 and 13:

(i) No matter any inclination angles, AE events can be divided into quiet period, low amplitude rising

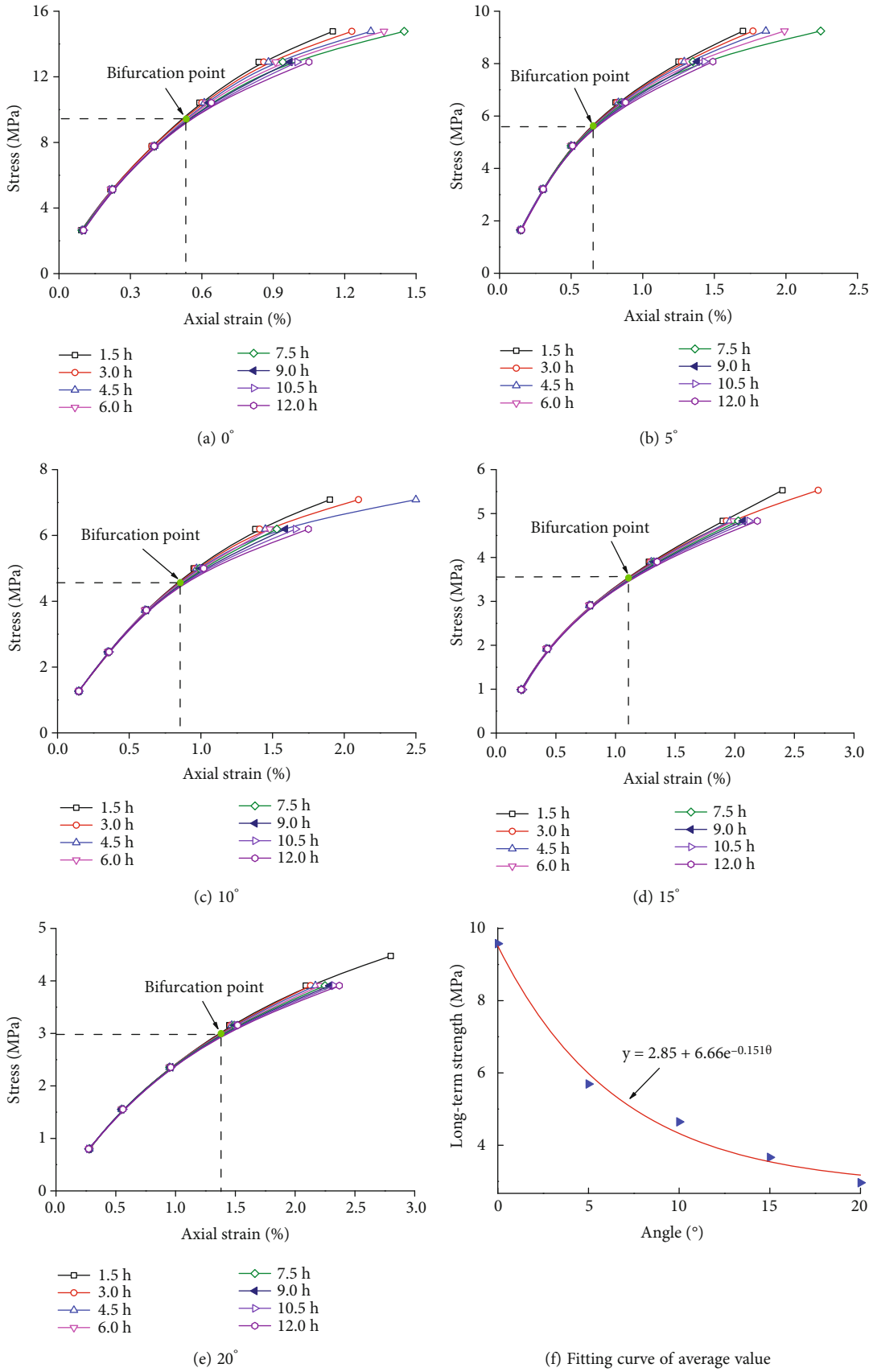

Figure 10: The LTS of coal specimens under various inclination angles.

Table 2: The LTS of coal specimens at different inclination angles.

Inclination angles		Long-term strength (MPa)	Average value (MPa)	Absolute deviation (MPa)	Relative deviation (%)	Standard deviation (MPa)	Relative standard deviation (%)
0°	1#	9.53	9.58	0.05	0.52	0.04	0.42
	2#	9.61		0.03	0.31		
	3#	9.59		0.01	0.10		
5°	1#	5.71	5.69	0.02	0.35	0.067	1.18
	2#	5.75		0.06	1.04		
	3#	5.62		0.07	1.25		
10°	1#	4.7	4.65	0.05	1.06	0.06	1.29
	2#	4.58		0.07	1.53		
	3#	4.66		0.01	0.21		
15°	1#	3.69	3.66	0.03	0.81	0.08	2.18
	2#	3.57		0.09	2.52		
	3#	3.73		0.07	1.88		
20°	1#	2.97	2.96	0.01	0.34	0.02	0.67
	2#	2.94		0.02	0.68		
	3#	2.98		0.02	0.67		

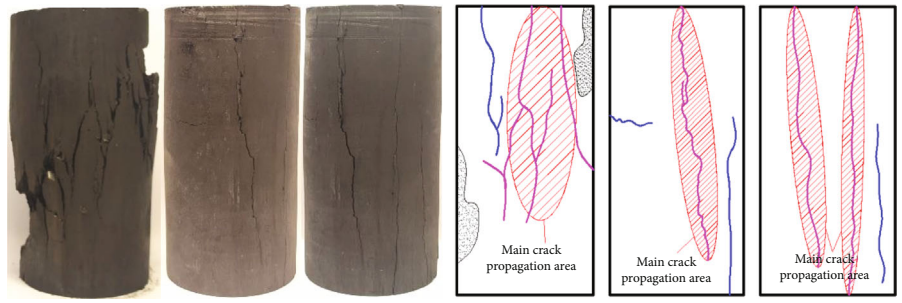

(a) 0°

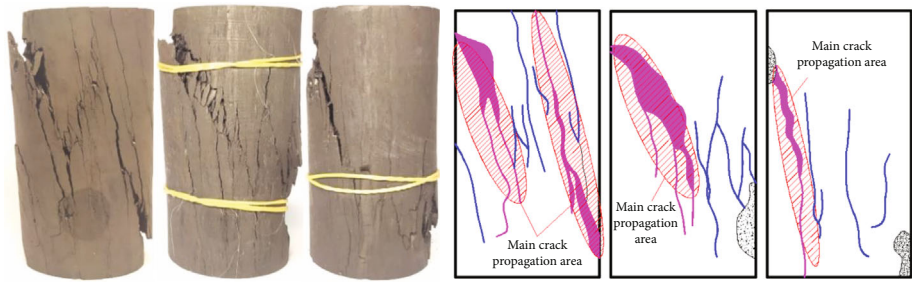

(b) 5°

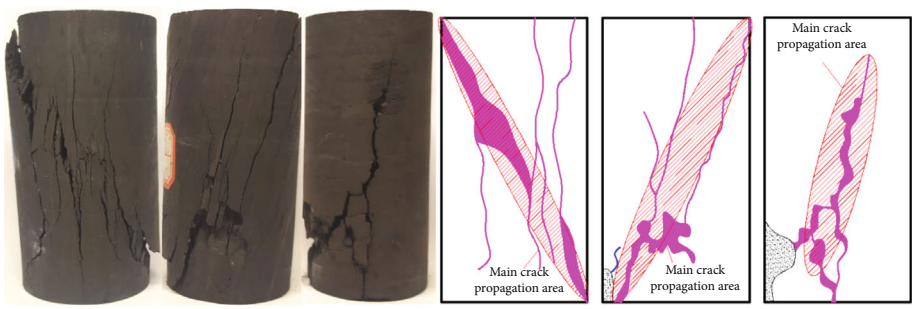

(c) 10°

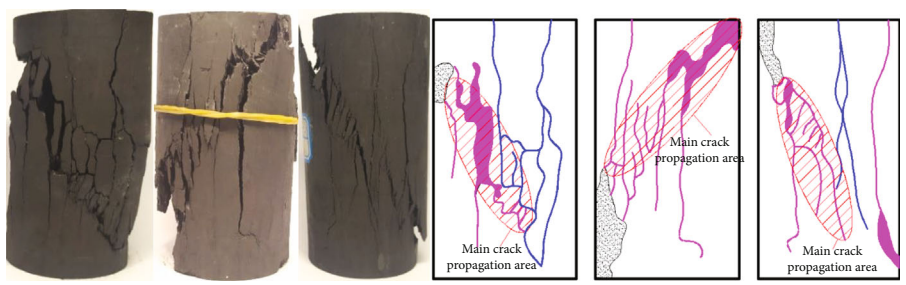

(d) 15°

Figure 11: Continued.

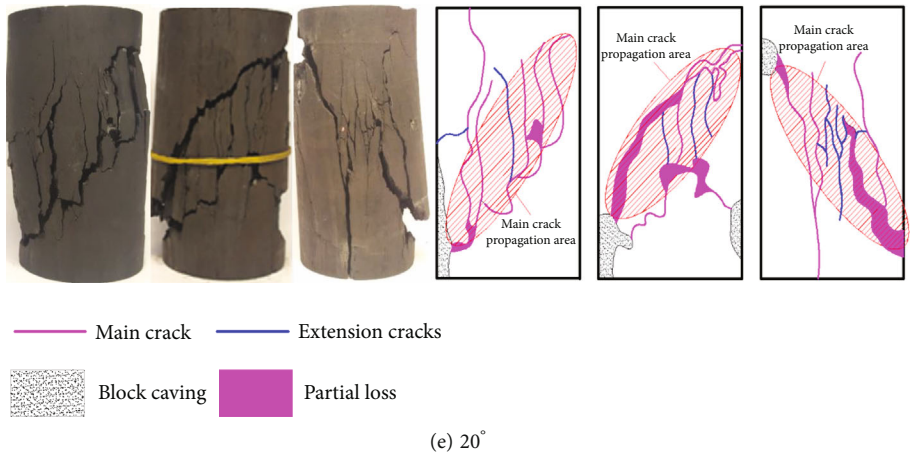

(e) 20°

Figure 11: Fracture photographs of coal specimens at various inclination angles.

period, and high amplitude rising period with the periodic mutation of multistage loading points

(ii) The AE quiet period accounts for the elastic strain energy accumulation in the process of creep test, during which the stress loading level is between $17\%\sigma_{max}$ and $33\%\sigma_{max}$. In this stage, the internal natural cracks close gradually, while the external loading level has not reached the threshold for crack initiation. Thus, the specimens can only release a small amount of energy when applied instantaneous loadings

(iii) The AE low amplitude rising period accounts for the crack initiation and propagation, during which the stress level is between $50\%\sigma_{max}$ and $83\%\sigma_{max}$ if the inclination angle changes from 0° to 5°. Additionally, the loading level is between $50\%\sigma_{max}$ and $67\%\sigma_{max}$ if the inclination angle changes from 10° to 20°. In this stage, the accumulative AE energy increases at a relatively low rate, indicating that the cracks start to initiate in the specimens under constant external loading at each level

(iv) The AE high amplitude rising period accounts for the propagation and penetration of cracks, under which the stress level is $95\%\sigma_{max}$ if the inclination angle changes from 0° to 5°. Besides that, the loading level is between $83\%\sigma_{max}$ and $95\%\sigma_{max}$ if the inclination angle changes from 10° to 20°. In this stage, the accumulative AE energy curve, with a relatively high increased rate, shows a distinct inflection point changed from the low amplitude rising period to the high amplitude rising period. It means that the specimens release large amounts of deformation energy, indicating that the cracks have propagated and start to rapidly coalesce

(v) The total accumulative AE energy decreases nonlinearly with the increase of inclination angles, indicating that the shear stress caused by inclination angle can cause crack initiation and propagation with less energy absorption

Starr [34] deduced the formula of average relative shear displacement between two cracks under the shear stress, which is expressed as

$$U_s = \pi(1-\nu)S \cdot \frac{c}{2G}, \tag{2}$$

where G and ν refer to the shear modulus and Poisson's ratio, respectively; c and S refer to the length of cracks and shear stress, respectively. Then, Starr described the relationship between the reduction of elastic strain energy and shear stress during the crack propagation process based on Equation (2), which is expressed as

$$W_e = \pi(1-\nu)S^2 \cdot \frac{c^2}{2G}. \tag{3}$$

Equation (3) indicates that the reduction of elastic strain energy is proportional to the square of shear stress, meaning that higher shear stress releases lesser AE energy. Chen [10] performed IUCS tests on yellow sandstones under various inclination angles using the IUCS test system. The results showed that shear stress in the specimens gradually increases with inclination angles, while the AE energy released by specimens under large inclination angles decreases. This phenomenon is basically consistent with the experimental results in this study.

4. Discussion

Above analyses indicate that the creep property of coal pillars is not only impacted by various factors such as the stress level, temperature, and moisture but also the pattern of the external loadings. Suorineni et al. [20] showed a negative correlation between pillar strength and inclination angles, believing that the shear stress component induced by inclination angle is the primary reason for pillar strength

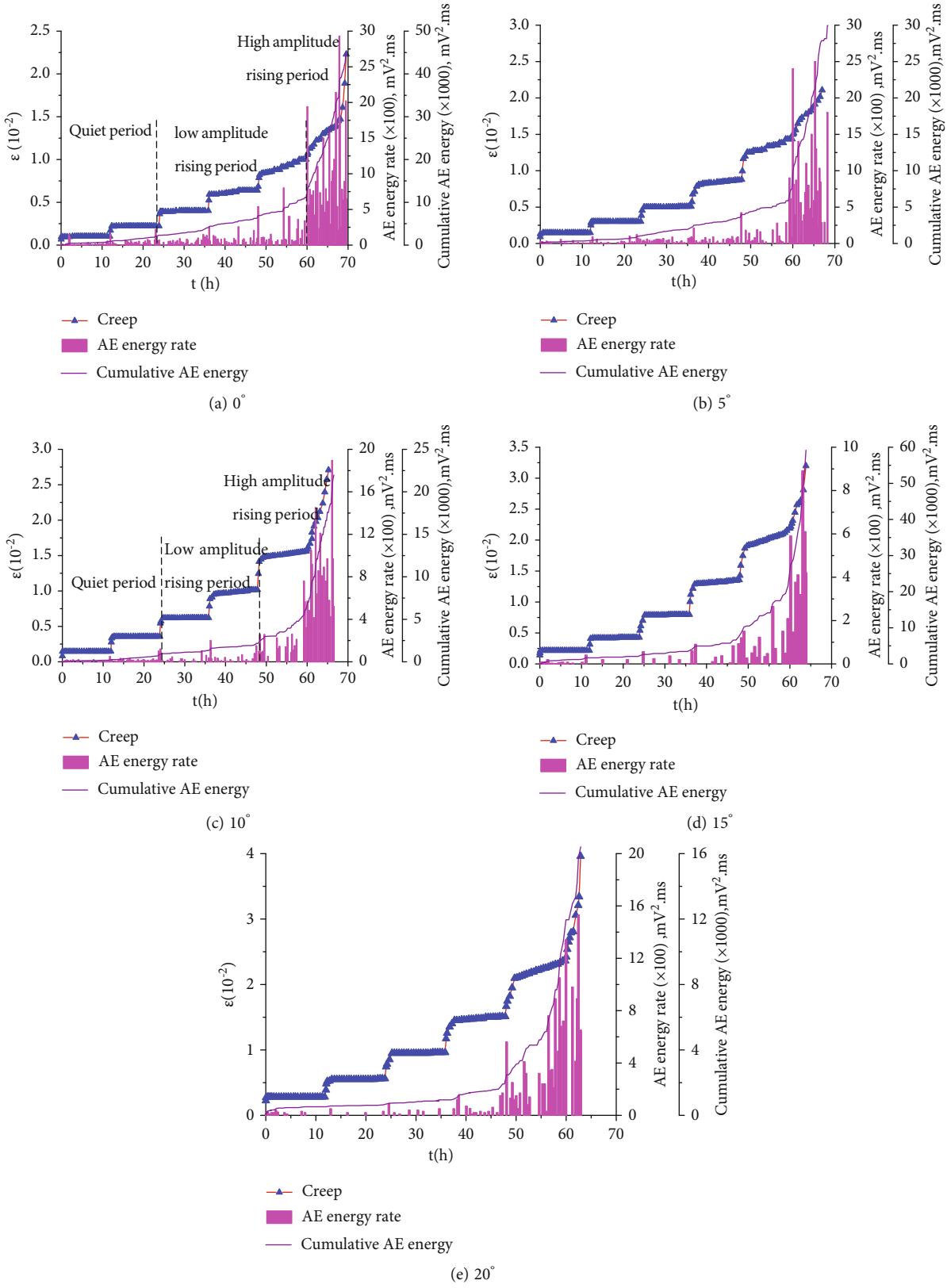

Figure 12: Relationship between AE energy and creep strain of coal specimens under various inclination angles.

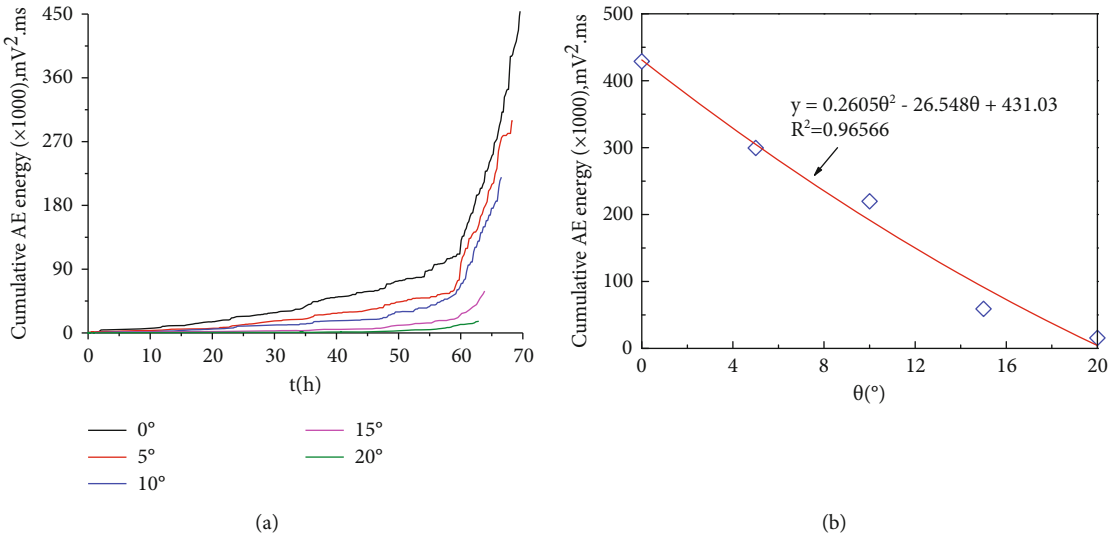

Figure 13: Variation of accumulative AE energy with (a) time and (b) inclination angles.

attenuation, which was agreed by Ma et al. [35]. If the coal pillar is vertical, coal specimens are under pure uniaxial compression, where the direction of external loading is parallel to the specimen axis. The coal specimens are mainly subject to compressive stress and few to shear stress. Therefore, only a higher stress level can lead to the crack initiating and propagating, suggesting a robust LTS of specimens. In this circumstance, the creep failure tends to exhibit a tensile-splitting mode. As the inclination angle increases, the angle between the external loading direction and specimen axis increases accordingly. It hence leads to an enhancement of the shear stress component. Resultantly, internal cracks can initiate and propagate under a lower stress level, leading to the LTS of specimens gradually declining. The previous tensile-splitting failure mode (0° to 5°) evolves to a composed mode (10° to 20°), incorporating shear failure as the primary and splitting failure as the auxiliary. Therefore, it suggests that the inclination effect on coal pillars should be considered in the LTS design.

There is a remarkable correlation between the accumulative AE energy and LTS: the energy attenuates with the strength declines. At lower inclination angles, the specimen fails as a tensile-splitting mode dominated by compressive stress with higher LTS. During the creep test, the initiation and propagation of cracks have to overcome the cohesive effect between particles within the coals at higher stress levels. Hence, the energy released after the failure is more remarkable. As the inclination angle increases, more shear stress occurs in the specimens, further weakening the LTS of coals, making it easier to reach the cracking threshold even under a lower stress level. Therefore, the specimens release lesser energy after the failure at high inclination degrees.

5. Conclusions

Based on the self-developed IUCS test system, this study performs a series of uniaxial compression tests and uniaxial creep tests on coal specimens under various inclination angles. It is aimed at investigating the effect of inclination angle on the creep failure behavior and macroscopic cracking characteristics. Additionally, we also study the energy release rule in the multistage creep process by using the AE technique. The main conclusions are as follows:

(i) The axial creep strain characteristics are the same when the inclination angles are different. When the stress level is below 83%σ_{max}, the creep curves have only two creep stages: the primary and steady stages. When the level is 95%σ_{max}, the creep curves show three creep stages: the primary-steady-accelerated creep stages. The critical accelerated creep strain increases linearly with the increase of inclination angles, while the creep time when specimens fail decreases linearly

(ii) The LTS of coal specimens attenuates nonlinearity with the inclination angle increases, suggesting that the LTS of coal pillars can be weakened due to their inclination. Hence, the inclination angle should be considered for designing the LTS of coal pillars. The proportion of the peak strength to the LTS had remained constant between 58.5% and 62.9%, which can be considered as the inherent properties of coal rock

(iii) The inclination angles significantly impact the creep failure modes and the degree of fragmentation specimens. The failure modes gradually transform from the pure tensile-splitting mode (0° and 5°) to a combination model of both splitting and shear sliding (10°-20°) with increasing inclination angles

(iv) Under any inclination angles, AE events during the creep test can be divided into quiet period, low amplitude rising period, and high amplitude rising period. The total accumulative AE energy decreases nonlinearly with the increase of inclination angles,

indicating that the shear stress can cause crack initiation and propagation with less energy absorption. The total accumulative AE energy of coal specimens is also highly correlated to their LTS; the lower the long-term strength, the lesser the AE energy released

Data Availability

All the data used to support the findings of this study are included with in the article.

Conflicts of Interest

There are no conflicts of interest regarding the publication of this paper.

Acknowledgments

The study was supported by the National Natural Science Foundation of China (51874277).

References

[1] S. Y. Zhang, G. W. Fan, Q. Z. Li, S. Z. Zhang, and L. Chen, "Effect of mining parameters on surface deformation and coal pillar stability under customized shortwall mining of deep extra-thick coal seams," *Energy Reports*, vol. 7, no. 409, pp. 2138–2154, 2021.

[2] Y. Cao, L. Chen, P. Wu, and F. Shaikh, "Experimental study on granite acoustic emission and micro-fracture behavior with combined compression and shear loading: phenomenon and mechanism," *Scientific Reports*, vol. 10, no. 1, pp. 1–7, 2020.

[3] C. Zhang, F. Wang, and Q. Bai, "Underground space utilization of coalmines in China: a review of underground water reservoir construction," *Tunnelling and Underground Space Technology*, vol. 107, article 103657, 2021.

[4] B. F. Wang, B. Liang, J. G. Wang et al., "Experiment study on rock bulking of coal mine underground reservoir," *Rock and Soil Mechanics*, vol. 39, no. 11, pp. 4086–4092, 2018.

[5] F. T. Wang, N. Liang, and G. Li, "Damage and failure evolution mechanism for coal pillar dams affected by water immersion in underground reservoirs," *Geofluids*, vol. 2019, no. 1, Article ID 2985691, 2019.

[6] P. J. Lunder, *Hard Rock Pillar Strength Estimation: An Applied Approach, [M.S. Thesis]*, University of British Columbia, Vancouver, 1994.

[7] W. A. Hustrulid, "A review of coal pillar strength formulas," *Rock Mechanics and Rock Engineering*, vol. 8, no. 2, pp. 115–145, 1976.

[8] J. N. Van der Merwe and M. Mathey, "Update of coal pillar strength formulae for South African coal using two methods of analysis," *Journal of the Southern African Institute of Mining and Metallurgy*, vol. 113, no. 11, pp. 841–847, 2013.

[9] C. Wei, C. G. Zhang, I. Canbulat, and W. Huang, "Numerical investigation into impacts of major fault on coal burst in longwall mining - a case study," *International Journal of Rock Mechanics and Mining Sciences*, vol. 147, article 104907, 2021.

[10] L. Chen, P. Wu, Y. Chen, and W. Zhang, "Experimental study on physical-mechanical properties and fracture behaviors of saturated yellow sandstone considering coupling effect of freeze-thaw and specimen inclination," *Sustainability*, vol. 12, no. 3, p. 1029, 2020.

[11] W. G. Pariseau, "Shear stability of mine pillars in dipping seams," in *American Rock Mechanics Association*, American Rock Mechanics Association, 1982.

[12] A. J. Das, P. K. Mandal, P. S. Paul, R. K. Sinha, and S. Tewari, "Assessment of the strength of inclined coal pillars through numerical modelling based on the ubiquitous joint model," *Rock Mechanics and Rock Engineering*, vol. 52, no. 10, pp. 3691–3717, 2019.

[13] R. Hou, L. Xu, D. Zhang, Y. Shi, and L. Shi, "Experimental investigations on creep behavior of coal under combined compression and shear loading," *Geofluids*, vol. 2021, no. 2, Article ID 9965228, 2021.

[14] A. Sainoki and H. S. Mitri, "Numerical investigation into pillar failure induced by time-dependent skin degradation," *International Journal of Mining Science and Technology*, vol. 27, no. 4, pp. 591–597, 2017.

[15] S. J. Chen, W. J. Guo, G. Q. Cheng, and T. P. Zhao, "Research on creep supporting effect of deep strip pillar," *Journal of Mining & Safety Engineering*, vol. 29, no. 9, pp. 48–53, 2012.

[16] B. Mishra and P. Verma, "Uniaxial and triaxial single and multistage creep tests on coal-measure shale rocks," *International Journal of Coal Geology*, vol. 137, no. 1, pp. 55–65, 2015.

[17] Y. Yang, D. Wang, N. Zhao, and S. Chen, "Acoustic emission characteristics of coal creep under step load," *Yingyong Jichu yu Gongcheng Kexue Xuebao/Journal of Basic ence and Engineering*, vol. 21, no. 1, pp. 159–166, 2013.

[18] S. Q. Yang, P. Xu, and T. Xu, "Nonlinear visco-elastic and accelerating creep model for coal under conventional triaxial compression," *Geomechanics & Geophysics for Geo-Energy & Geo-Resources*, vol. 1, no. 3-4, pp. 109–120, 2015.

[19] M. H. Foroughi and V. S. Vutukuri, "Estimating elastic pillar stresses in inclined coal seams," *Transaction of Society for Mining, Metallurgy and Exploration*, vol. 302, pp. 50–54, 1997.

[20] F. T. Suorineni, J. J. Mgumbwa, P. K. Kaiser, and D. Thibodeau, "Mining of orebodies under shear loading part 2 -failure modes and mechanisms," *Mining Technology IMM Transactions Section A*, vol. 123, no. 4, pp. 240–249, 2014.

[21] H. Wu, H. Bai, Y. Chen, H. Pu, and K. Zhang, "Mechanical properties and damage in lignite under combined cyclic compression and shear loading," *Sustainability*, vol. 12, no. 20, p. 8393, 2020.

[22] Q. Y. He, Y. C. Li, D. Q. Li, and C. G. Zhang, "Microcrack fracturing of coal specimens under quasi-static combined compression-shear loading," *Journal of Rock Mechanics and Geotechnical Engineering*, vol. 12, no. 5, pp. 1014–1026, 2020.

[23] Y. L. Chen, H. D. Cui, H. Pu, P. Wu, and K. Zhang, "Study on mechanical properties and cracking mode of coal samples under compression–shear coupled load considering the effect of loading rate," *Applied Sciences*, vol. 10, no. 20, p. 7082, 2020.

[24] P. Wu, L. Chen, Y. L. Chen et al., "Experimental study on mechanical properties and microcrack fracture of coal specimens under the coupling of loading rate and compression-shear loads," *International Journal of Geomechanics*, vol. 22, no. 4, 2022.

[25] P. Hou, X. Liang, F. Gao, J. B. Dong, J. He, and Y. Xue, "Quantitative visualization and characteristics of gas flow in 3D pore-fracture system of tight rock based on lattice Boltzmann simulation," *Journal of Natural Gas Science and Engineering*, vol. 89, article 103867, 2021.

[26] P. Hou, X. Liang, Y. Zhang, J. He, F. Gao, and J. Liu, "3D multi-scale reconstruction of fractured shale and influence of fracture morphology on shale gas flow," *Natural Resources Research*, vol. 30, no. 3, pp. 2463–2481, 2021.

[27] X. Liang, P. Hou, Y. Xue, X. J. Yang, F. Gao, and J. Liu, "A fractal perspective on fracture initiation and propagation of reservoir rocks under water and nitrogen fracturing," *Fractals*, vol. 29, no. 7, 2021.

[28] X. Liang, P. Hou, X. J. Yang et al., "On estimating plastic zones and propagation angles for mixed mode I/II cracks considering fractal effect," *Fractals*, vol. 30, no. 1, 2022.

[29] P. Hou, S. J. Su, X. Liang et al., "Effect of liquid nitrogen freeze-thaw cycle on fracture toughness and energy release rate of saturated sandstone," *Engineering Fracture Mechanics*, vol. 258, article 108066, 2021.

[30] Y. Zhang, P. J. Jin, W. Y. Xu, H. B. Zhao, and S. H. Mei, "Experimental study of triaxial creep behavior and long-term strength of clastic rock in dam foundation," *Rock and Soil Mechanics*, vol. 37, no. 5, pp. 1291–1300, 2016.

[31] M. R. Shen and H. J. Chen, "Testing study of long-term strength characteristics of red sandstone," *Rock and Soil Mechanics*, vol. 32, pp. 3301–3305, 2011.

[32] Z. W. Zhou, W. Ma, S. J. Zhang, H. M. Du, Y. H. Mu, and G. Y. Li, "Multiaxial creep of frozen loess," *Mechanics of Materials*, vol. 95, pp. 172–191, 2016.

[33] R. B. Hou, K. Zhang, and J. Tao, "Effects of initial damage on time-dependent behavior of sandstone in uniaxial compressive creep test," *Archives of Mining Sciences*, vol. 64, no. 4, pp. 687–707, 2019.

[34] A. T. Starr, "Slip in a crystal and rupture in a solid due to shear," *Mathematical Proceedings of the Cambridge Philosophical Society*, vol. 24, no. 4, pp. 489–500, 1928.

[35] T. Ma, L. Wang, F. T. Suorineni, and C. Tang, "Numerical analysis on failure modes and mechanisms of mine pillars under shear loading," *Shock and Vibration*, vol. 2016, 14 pages, 2016.